ADVANCING EARTH AND SPACE SCIENCE

Geophysical Research Letters®

RESEARCH LETTER
10.1029/2021GL094035

Temperature-Regulated Turnover of Chromophoric Dissolved Organic Matter in Global Dark Marginal Basins

Chao Wang[1,2], Weidong Guo[1], Yan Li[3], Randy A. Dahlgren[4], Xianghui Guo[1], Liyin Qu[1], and Wei Zhuang[1]

[1]State Key Laboratory of Marine Environmental Science, College of Ocean and Earth Sciences, Xiamen University, Xiamen, China, [2]College of Ocean and Meteorology, Guangdong Ocean University, Zhanjiang, China, [3]Dongshan Swire Marine Station, Xiamen University, Xiamen, China, [4]Department of Land, Air and Water Resources, University of California, Davis, CA, USA

Key Points:

- Faster turnover for optical components of dissolved organic matter (DOM) was observed in dark marginal basins than in the open ocean
- In situ production efficiency of two ubiquitous humic-like fluorophores increased at higher dark ocean temperatures
- An increase of DOM recalcitrance and decrease of the bulk dissolved organic carbon pool may occur due to a future warming of dark basins

Supporting Information:

Supporting Information may be found in the online version of this article.

Correspondence to:

W. Guo,
wdguo@xmu.edu.cn

Citation:

Wang, C., Guo, W., Li, Y., Dahlgren, R. A., Guo, X., Qu, L., & Zhuang, W. (2021). Temperature-regulated turnover of chromophoric dissolved organic matter in global dark marginal basins. *Geophysical Research Letters*, *48*, e2021GL094035. https://doi.org/10.1029/2021GL094035

Received 23 APR 2021
Accepted 8 SEP 2021

Abstract

Oceanic absorption of heat generated by greenhouse gas emissions has resulted in warming of the dark ocean (>200 m) that contains a large refractory DOM (RDOM) pool. However, changes in microbially mediated production and degradation dynamics for RDOM components in response to warming of dark marginal basins remain unclear. Herein, we integrated data from the dark South China, Mediterranean and Japan Seas (temperature range: 0.09–15.1°C) to demonstrate that in situ production efficiency of two ubiquitous humic-like fluorophores increased at higher dark ocean temperature, whereas chromophores at a wavelength of 325 nm ($a_{CDOM}(325)$) changed from production to degradation at higher temperature. Increased oxygen consumption and a reduction of labile substrates in future warmer dark ocean environments may initiate the final degradation of some semi-refractory components, thereby increasing the recalcitrance of RDOM, but decreasing the DOM inventory in dark basins and creating a positive feedback to rising atmospheric CO_2.

Plain Language Summary

Marine refractory dissolved organic matter (RDOM) in the dark ocean is primarily formed during heterotrophic degradation of labile organic matter, which has a pronounced sensitivity to temperature variation. Since the 1960s, the global dark ocean has exhibited an accelerated warming with a discernable temperature increase. Thus, determining the importance of temperature on microbial regulation of the oceanic RDOM pool is of great significance. This study utilized the ocean interior of the marginal South China, Mediterranean and Japan Seas as natural basin-scale enclosed incubators along with optical DOM characterization methods to reveal a production-degradation reaction series for RDOM components. A decrease in the DOM inventory by enhanced microbial mineralization (producing CO_2) in a warmer dark ocean may create a positive feedback in response to global climate change.

1. Introduction

Marine dissolved organic matter (DOM) in the dark ocean (>200 m) contains a large refractory DOM (RDOM) pool (~615 Pg carbon) similar in magnitude to the atmospheric CO_2-C pool (Hansell, 2013). The RDOM pool is primarily formed during heterotrophic degradation of labile organic matter, which has a pronounced sensitivity to temperature (Brewer & Peltzer, 2017; Jiao et al., 2010; Shen & Benner, 2020). Since the 1960s, the ocean has exhibited an accelerated warming at all depths, with a discernable temperature increase in the global dark ocean (Cheng et al., 2017; Levitus et al., 2012). Thus, determining the temperature effect on microbial regulation of the oceanic RDOM pool is essential as its carbon exchange with the atmosphere is a potentially sensitive feedback mechanism to global climate change (Lønborg et al., 2020). However, detailed knowledge concerning the temperature sensitivity of the RDOM pool is still lacking (Lønborg et al., 2018).

The semi-enclosed nature and distinctive geomorphology of dark marginal basins create unique ventilation and circulation patterns relative to the open ocean interior that strongly alter the export flux of degradable organic matter and oxygen utilization (Kim et al., 2011; Qu et al., 2006; Santinelli, 2015; Shen, Jiao, et al., 2020). Thus, marginal basins may have distinctly different warming effects on microbial transformation of RDOM components compared with the dark open ocean (Catalá, Reche, Fuentes-Lema, et al., 2015).

We posit that the response of RDOM cycling dynamics to warming in dark marginal basins could be highly sensitive as future temperature increases in some dark marginal basins are projected to be higher than in the dark open ocean (Soto-Navarro et al., 2020).

In situ specific transformation efficiency of RDOM per unit oxygen consumption can be estimated by relationships between chromophoric DOM (CDOM) and its fluorescence components (FDOM) with apparent oxygen utilization (AOU), after accounting for water mass mixing signals (Swan et al., 2009). Once oxygen utilization rates (OUR) in the dark oceans are available, in situ transformation rates of RDOM components can be quantified and their turnover times determined (Catalá, Reche, Álvarez, et al., 2015; Catalá, Reche, Fuentes-Lema, et al., 2015). Herein, we investigated vertical profiles of CDOM ($a_{CDOM}(254)$; $a_{CDOM}(325)$), tryptophan-like peak T ($FDOM_T$), and humic-like peaks A and M (together $FDOM_H$) in the dark northern South China Sea (SCS) and integrated our data with literature data from the dark East/West Mediterranean (Med) Sea, Japan Sea and global ocean (Catalá et al., 2018; Kim & Kim, 2016; Martínez-Pérez et al., 2019; Tanaka et al., 2014). The ocean interiors of the three marginal basins provide natural basin-scale enclosed 'incubators' comprising a suitable temperature range (0.09–15.1°C) to evaluate temperature effects on in situ turnover rates and production-degradation dynamics for RDOM components. The future change of in situ $FDOM_H$ production efficiency/rates in the dark marginal basins under the moderate greenhouse gas emission scenario (RCP4.5) by the end of the 21st century was projected to illustrate the potential impacts on RDOM components.

2. Materials and Methods

2.1. Dark South China Sea (SCS)

Water samples were collected at 33 stations using 10-L Niskin bottles attached on a Rosette sampler from May 20 to June 5, 2016 and June 20 to July 9, 2018 for the northern SCS, Luzon Strait and adjacent Northwest Pacific (Figure S1a). Temperature and salinity profiles were obtained using a calibrated SBE 911plus CTD unit. Apparent oxygen utilization (AOU) was calculated as the difference between the saturation and measured DO concentration using Winkler methods (Benson & Krause, 1984).

Samples for CDOM and FDOM analyses were filtered through precombusted 0.7 μm GF/F filters (Whatman) and the filtrate stored at 4°C until analysis back on land within three weeks from the beginning of sampling (Coble et al., 2014). CDOM absorption was determined from 240 to 800 nm using a 2310 UV-Visible spectrophotometer (Techcomp, China) against an ultrapure Milli-Q water blank (Wang et al., 2017). Fluorescence excitation-emission matrices (emission scan: 280–600 nm, excitation scan: 240–450 nm) normalized to Raman Units (RU) were measured using a Varian Cary Eclipse spectrofluorometer (Agilent, USA) for May–June 2016 samples and a F-7100 spectrofluorometer (Hitachi, Japan) for June–July 2018 samples (Wang et al., 2017). The ubiquitous two humic-like (peak A, ex/em: 260/456 nm, and peak M, ex/em: 320/400 nm) and one protein-like component (peak T, ex/em: 275/340 nm) were determined in this study (Coble, 1996; Wang et al., 2021) (Figure S2). The coefficients of variation for RU-normalized fluorescent intensities of the three peaks between the two spectrofluorometers for 5 samples collected during July 2018 cruise were <4%. Dissolved organic carbon (DOC) data from the SCS are available from Wu et al. (2015).

The net (Δ) non-conservative changes (i.e., biogeochemical addition or removal) of AOU, CDOM, and FDOM in the dark SCS was estimated based on a diapycnal three-end-member mixing analysis (Cao & Dai, 2011; Chen et al., 2001; Karstensen & Tomczak, 1998; Zhu et al., 2019) (Text S1, Figures S3 and S4). OUR (μmol kg^{-1} yr^{-1}) at a given depth is the oxygen consumption magnitude during the water renewal time (Liu & Gan, 2017) (Text S1). The positive or negative slopes of the linear relationship between ΔCDOM and ΔFDOM with ΔAOU were taken as the microbial production or degradation efficiency during mineralization-related transformations. The net in situ production or degradation rates of CDOM or FDOM components in the intermediate and deep SCS (m^{-1} yr^{-1} for CDOM and RU yr^{-1} for FDOM) were quantified from the calculated efficiencies and OUR. The turnover time for DOM optical components (Γ_C, in years) in the dark SCS was defined as the time required to produce the actual inventories by in situ production processes (Text S1).

2.2. Literature and Open-Source Data for the Dark Med and Japan Seas

Potential temperature and salinity data for the Med and Japan Seas are available from the WOA13 and GLODAPv2 data sets (https://odv.awi.de/data/ocean/). AOU and DOC in the Med Sea are extracted from Santinelli et al. (2010), while CDOM and FDOM data are from Catalá et al. (2018) and Martínez-Pérez et al. (2019) (Figure S1b). AOU and FDOM data in the Japan Sea are from Tanaka et al. (2014) and Kim and Kim (2016) (Figure S1c), while DOC data are from Kim et al. (2017). Data acquisition and reprocessing are described in Text S2.

OUR data in the Med Sea are calculated as the ratio of AOU and water mass age, which was estimated by multiple transient tracers (Stöven & Tanhua, 2014). OUR data for the Japan Sea are extracted from Min et al. (2002) and Kim et al. (2010) (Text S2), while OUR data for the dark global ocean are directly sourced from Catalá, Reche, Álvarez, et al. (2015). The in situ production/degradation efficiencies, rates and turnover times of CDOM and FDOM for the intermediate and deep waters in the dark Med Sea and global ocean were recalculated based on literature data by Catalá, Reche, Fuentes-Lema, et al. (2015), Catalá, Reche, Álvarez, et al. (2015), Catalá et al. (2018), and Martínez-Pérez et al. (2019) (Text S2, Table S1). The in situ production/degradation efficiencies, rates and turnover times for FDOM in the dark Japan Sea were calculated using an OUR-inversed method (Text S2, Table S1).

Future warming of three dark marginal basins and the global dark ocean (except Arctic) was estimated as the potential temperature anomaly between the 2096–2100 and 2006–2010 time periods (Text S3, Table S2). Based on the projected magnitude of warming, changes in OUR and in situ $FDOM_H$ production efficiency and rates for the three dark marginal basins and global ocean were estimated (Table S3).

3. Results

3.1. Basin Differences in Distribution of Temperature, AOU, and OUR

The dark SCS had the largest vertical gradients of potential temperature (3.3°C km^{-1}) due to weak ventilation. In contrast, strong downward ventilation resulted in the dark Med and Japan Seas having little temperature variation (0.2–0.7°C km^{-1}), and the highest and lowest average potential temperatures, respectively (Figure 1a, Table S1) (Kim et al., 2004). The dark SCS had the largest AOU range and mean value compared with the dark Japan Sea and West/East Med Sea (Figure 1b, Table S1). Contrary to the small AOU variation in the Med Sea, the intermediate layer of the SCS and Japan Sea had a significantly larger AOU gradient than in the deep layer (t-test, $p < 0.05$). The maximal AOU values in the SCS occurred at the oxygen minimum layer (1,200–1,500 m). The ΔAOU in the dark SCS increased rapidly from 1.6 ± 7.9 μmol kg^{-1} at 200 m to a maximum of 35.9 ± 4.3 μmol kg^{-1} at ~800 m, and then decreased to 17.8 ± 1.3 μmol kg^{-1} at 3,818 m (Figure S5).

The OUR monotonously decreased with depth in the three basins (Figure 1c), with significantly higher average OUR in the intermediate layer than in the deep layer (t-test, $p < 0.05$, Table S1). The OUR in the SCS was significantly lower than in the Japan Sea in both layers (t-test, $p < 0.05$), while being generally higher than in the Med Sea (Table S1). Except for the West Med Sea, the OURs of intermediate layers in marginal basins were higher than in the global ocean (0.8 ± 0.4 μmol kg^{-1} yr^{-1}, t-test, $p < 0.05$). The OUR in deep layers of all marginal basins was higher than in the global ocean (0.28 ± 0.09 μmol kg^{-1} yr^{-1}, t-test, $p < 0.05$).

3.2. Variation of DOM Quantity and Quality Among the Three Marginal Basins

The DOC in dark SCS was generally higher than in dark Med Sea, but ~50% lower than in dark Japan Sea (Figure 1d). However, DOC at depths >2,800 m in the Med Sea was higher than in the SCS (Santinelli et al., 2010; Wu et al., 2015). The lowest minimum DOC (~36 μM) in the deep East Med Sea was slightly lower than those of the deep SCS and adjacent deep Atlantic, and ~30% lower than the minimum DOC (~55 μM) in the deep Japan Sea (Kim et al., 2017; Santinelli et al., 2010). The $a_{CDOM}(254)$ in the SCS was higher than the Med Sea, but its decreasing tendency with depth was distinctly weaker than in the Med Sea (Figure 1e). $FDOM_T$ showed a similar decreasing trend with depth in the three basins (Figure 1f). However, $FDOM_T$ in the dark SCS and Med Sea were significantly lower than in the Japan Sea, which also contained high concentrations of labile dissolved amino acids (Kim et al., 2017).

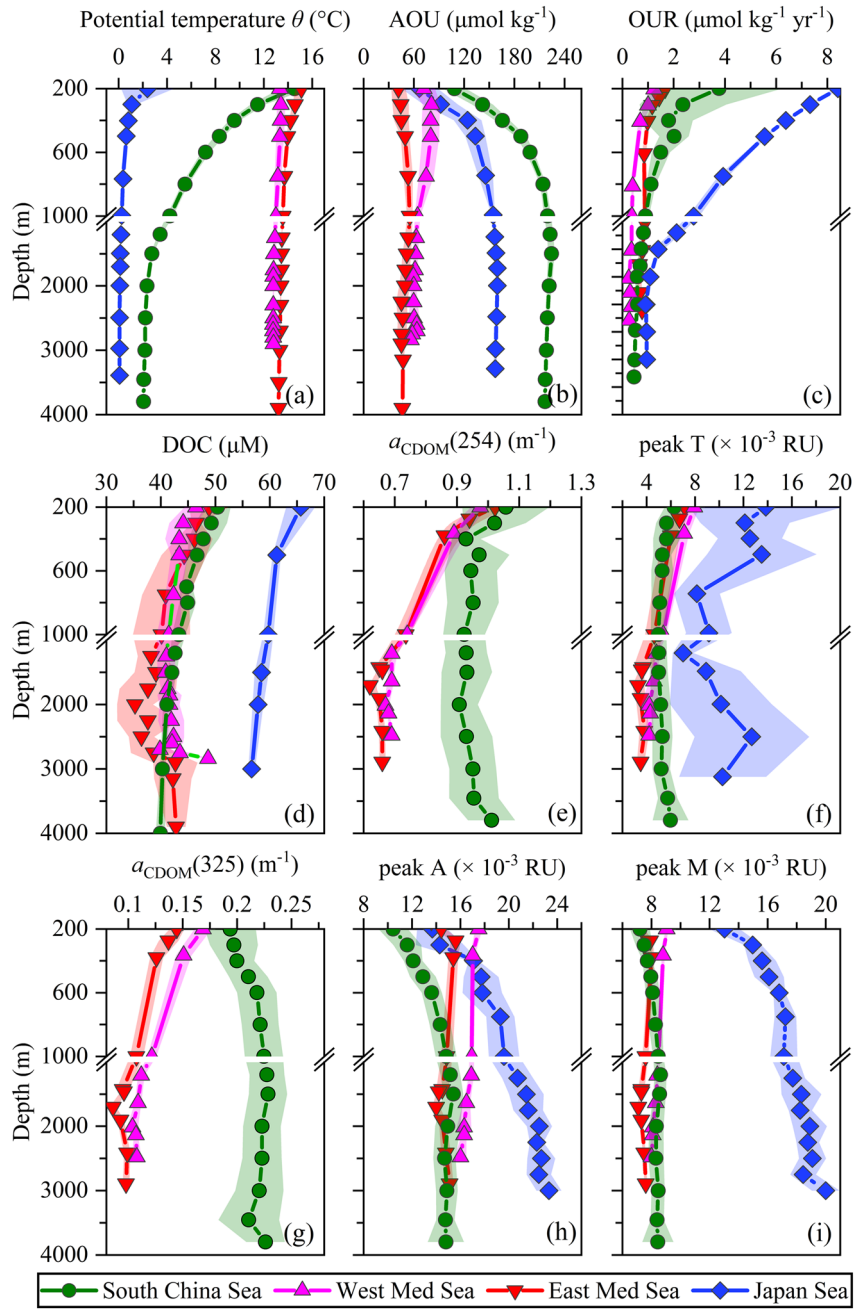

Figure 1. Profiles of hydrological, oxygen, and DOM parameters in dark South China Sea, West and East Mediterranean (Med) Seas and Japan Sea. (a) Potential temperature θ, (b) apparent oxygen utilization (AOU), (c) oxygen utilization rate (OUR), (d) DOC, (e) $a_{CDOM}(254)$, (f) peak T, (g) $a_{CDOM}(325)$, (h) peak A, and (i) peak M. Error bands represent standard deviations. Data sources are described in Text S1–S3.

The $a_{CDOM}(325)$ showed an increasing trend with depth in the SCS and was higher than in the adjacent Northwest Pacific (Figure S3g). In contrast, $a_{CDOM}(325)$ sharply decreased in the Med Sea (Figure 1g). Thus, $a_{CDOM}(325)$, DOC, $a_{CDOM}(254)$, and $FDOM_T$ in the deep layer of the Med Sea were generally lower than in the adjacent Northeast Atlantic (Hansell et al., 2009; Lønborg & Álvarez-Salgado, 2014). Similar to the open ocean, $FDOM_H$ increased with depth in the SCS and Japan Sea. Conversely, $FDOM_H$ showed a decrease with depth in the Med Sea (Figures 1h and 1i). Peak M in the SCS and Med Sea and peak A in deep SCS and Med Sea were significantly lower than in the Japan Sea (Figure 1i). However, peak A in the intermediate Med

Sea was higher than in the intermediate layers of the SCS. The $a_{CDOM}(325)$ and $FDOM_H$ in the West Med Sea were consistently higher than in the East Med Sea ($p < 0.05$, Figures 1g–1i, Table S1).

3.3. Relationships Between Net AOU and DOM Optical Components

Strong positive relationships between $\Delta FDOM_H$ and ΔAOU or archetypal $FDOM_H$ and archetypal AOU occurred for the intermediate SCS (200–1,000 m) ($p < 0.05$) (Figures 2a and 2b), as well as the intermediate Japan Sea (Figures 2f and 2g), Med Sea (except deep east basin, >1,000 m) (Figures 2i and 2j) and open ocean (Catalá, Reche, Álvarez, et al., 2015; Catalá, Reche, Fuentes-Lema, et al., 2015; Lønborg & Álvarez-Salgado, 2014). The positive relationships between $\Delta FDOM_H$ and ΔAOU were also significant in the deep SCS ($p < 0.05$) (Figures 2a and 2b). However, this contrasted with the accumulation pattern in the deep Japan Sea (Kim & Kim, 2016; Tanaka et al., 2014), and degradation pattern in the deep East Med Sea (Figures 2i and 2j). Similar to the open ocean (Catalá, Reche, Álvarez, et al., 2015), strong linear relationships between net $CDOM_{UVA}$ ($\Delta a_{CDOM}(325)$) and ΔAOU were observed in both the intermediate and deep SCS ($p < 0.05$) (Figure 2c). Notably, $a_{CDOM}(325)$ showed a negative correlation with archetypal AOU in the entire dark Med Sea (Figure 2k) (Catalá et al., 2018). Strong negative correlations between archetypal values of $a_{CDOM}(254)$, peak T and AOU were also observed in the intermediate Med Sea and deep West Med Sea ($p < 0.05$) (Figures 2l–2m). Similar strong negative correlations between Δpeak T and ΔAOU were observed in the intermediate Japan Sea ($p < 0.05$) (Figure 2h) and deep SCS ($p < 0.05$) (Figure 2e). There were no significant relationships between $\Delta a_{CDOM}(254)$, Δpeak T and ΔAOU in the intermediate SCS ($p > 0.05$) (Figures 2d and 2e).

The slopes of linear relationships between $\Delta FDOM_H$, $\Delta CDOM_{UVA}$, and ΔAOU (or between archetypal $FDOM_H$, $CDOM_{UVA}$, and archetypal AOU) represent the in situ production efficiency (or degradation if negative slopes) for $FDOM_H$ or $CDOM_{UVA}$ per unit of oxygen consumption (Catalá, Reche, Álvarez, et al., 2015; Catalá, Reche, Fuentes-Lema, et al., 2015; Hayase & Shinozuka, 1995; Yamashita & Tanoue, 2008). Notably, the slopes of the two $FDOM_H$ components showed a general increasing trend with increasing dark ocean temperature when including the marginal basins and open ocean data together. However, there was a slight positive deviation in the dark Japan Sea, and an abrupt reversal (i.e., from production to degradation) in the warmer deep east Med Sea (Figures 3a and 3b). In contrast, the slopes between $a_{CDOM}(325)$ and temperature were negative, and all dark Med Seas displayed consistent negative values for in situ production efficiency (Figure 3c).

3.4. In Situ Production/Degradation Rates and Turnover of $FDOM_H$ and $CDOM_{UVA}$ in Dark Marginal Basins

Net annual in situ production rates for $FDOM_H$ (except the deep East Med Sea) and $a_{CDOM}(325)$ (except the Med Sea) were quantified as the product of the specific production efficiency and OUR. Production rates showed large variations in marginal basins, but were all higher than that of the global ocean (*t*-test, $p < 0.05$, Table S1). In both intermediate and deep layers (assuming the deep Japan Sea has the same production efficiency as its intermediate layer), $FDOM_H$ production rates were highest in the dark Japan Sea, followed by the dark SCS and dark Med Sea (Table S1). This variation trend was generally opposite to that of the specific production efficiency.

Net annual in situ degradation rates for $a_{CDOM}(325)$ were quantified as the product of the specific degradation efficiency and OUR. In situ $a_{CDOM}(325)$ degradation rates were higher in the East Med Sea than in the West Med Sea for both intermediate and deep layers (*t*-test, $p < 0.05$, Table S1). Notably, the $FDOM_H$ degradation rates in the deep East Med Sea were higher than the $FDOM_H$ production rates in the West Med Sea (*t*-test, $p < 0.05$, Table S1).

For in situ production processes, turnover times for $FDOM_H$ and $a_{CDOM}(325)$ were defined as the time required to produce the actual inventories. Turnover times were shorter in intermediate marginal basins (46 ± 16–370 ± 92 years) than those in the intermediate global ocean (352 ± 113–546 ± 185 years) (*t*-test, $p < 0.05$, Table S1). The intermediate Japan Sea had the shortest turnover times, followed by the SCS, East and West Med Seas (Table S1). Turnover times in deep marginal basins (222 ± 40–710 ± 124 years) were shorter than those in the deep global ocean (Catalá, Reche, Álvarez, et al., 2015; Catalá, Reche,

10.1029/2021GL094035

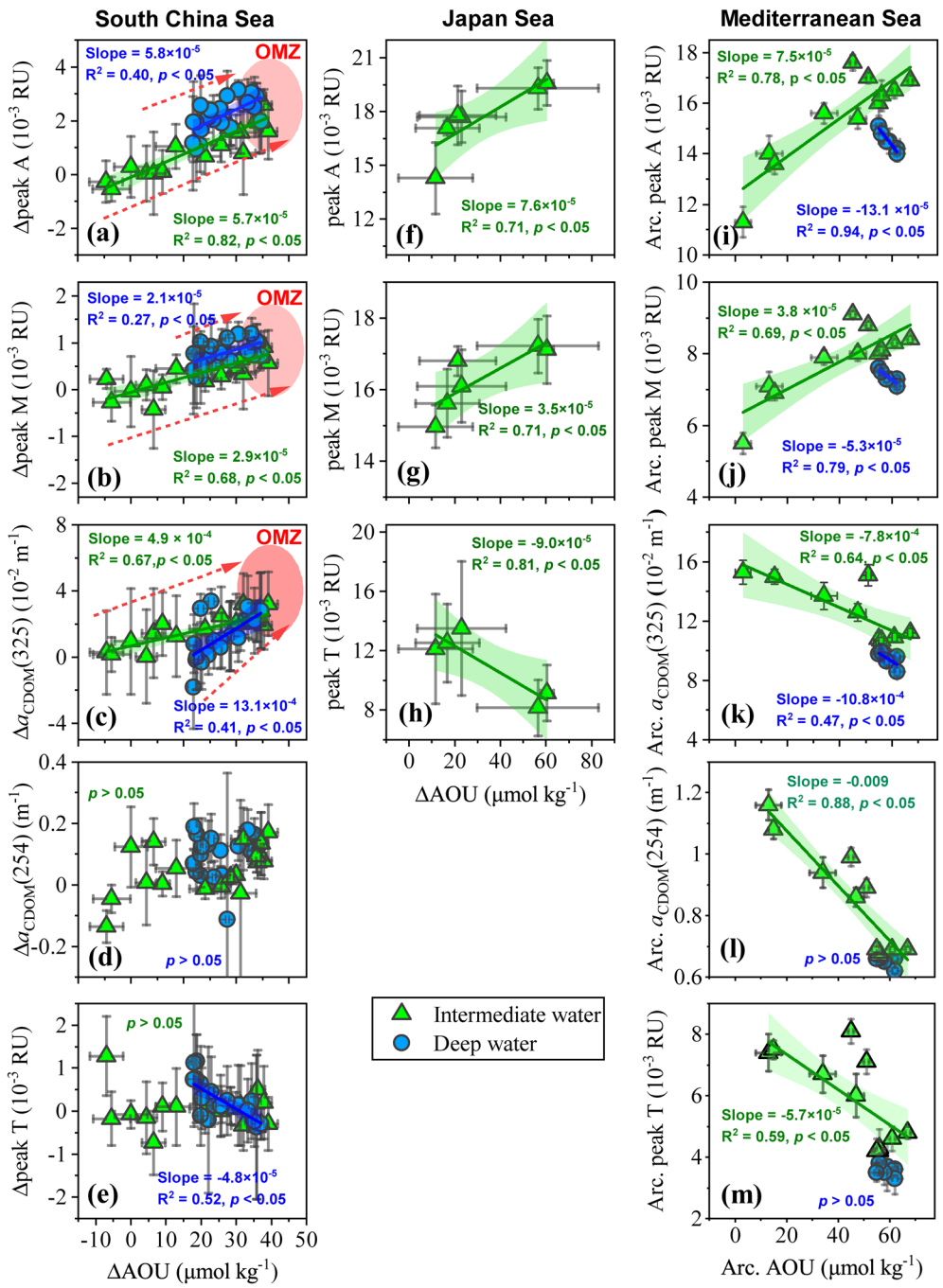

Figure 2. Comparisons of relationships between net (Δ) FDOM, CDOM, and AOU in the SCS (a–e) and Japan Sea (f–h) and between archetypal (Arc.) FDOM, CDOM, and AOU in the Mediterranean (Med) Sea (i–m). In panels (i–m), green triangles represent data of intermediate Med Sea and deep West Med Sea, and blue circles represent data from the East Med Sea. Points represent the averages at the specific depths for three individual regions of SCS (a–e), the dark Japan Sea (f–h), and for archetypal water types of Med Sea (i–m). Error bars represent the standard deviations. Solid lines represent the linear regressions with the 95% confidence intervals indicated by light shading. The ΔAOU data at the 200 m depth in the Japan Sea were excluded from the linear regression analyses (Text S2). Data source and reprocessing are described in Text S1–S3. OMZ, oxygen minimum zone.

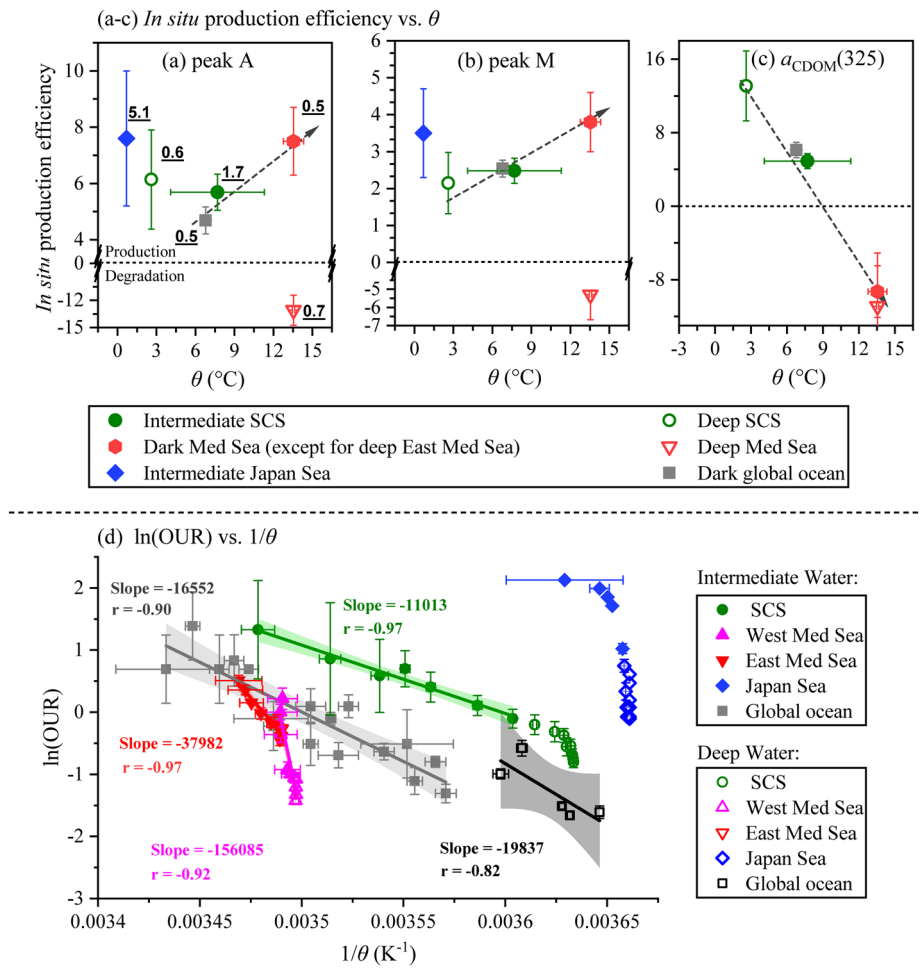

Figure 3. Relationships between the in situ production efficiency of (a) humic-like peak A, (b) peak M, (c) a_{CDOM}(325) with potential temperature θ (unit: °C), and (d) Van't Hoff/Arrhenius relationships between OUR (unit: μmol kg^{-1} yr^{-1}) and potential temperature θ (unit: K) in the dark South China Sea (SCS), Mediterranean (Med) Sea, Japan Sea, and global ocean (>200 m). The in situ production efficiencies (unit: 10^{-5} RU/(μmol kg^{-1} O_2) for peak A and peak M; 10^{-4} m^{-1}/(μmol kg^{-1} O_2) for a_{CDOM}(325)) are the slopes of linear relationships between net or archetypal DOM optical parameters with AOU (Figure 2, Text S1–S3). The number associated with each point in panel (a) represents the average OUR (unit: μmol kg^{-1} yr^{-1}) for the specific layer. Negative in situ production efficiency means net degradation. Error bars represent the standard deviations.

Fuentes-Lema, et al., 2015) (1,160 ± 150–1,557 ± 168 years) (*t*-test, $p < 0.05$, Table S1), with much faster turnover times in the deep SCS and Japan Sea than in the deep West Med Sea. In the dark Japan Sea, turnover times for $FDOM_H$ were much lower than the water renewal time (~1,000 years) (Watanabe et al., 1991). Conversely, turnover times for $FDOM_H$ and $CDOM_{UVA}$ in the dark SCS and Med Sea were longer than the water renewal times for the dark SCS (<50 years) and Med Sea (<150 years).

For in situ degradation processes, the turnover time for a_{CDOM}(325) was defined as the time required to consume the entire inventory. The a_{CDOM}(325) turnover times were shorter in the East Med Sea (126 ± 69–133 ± 47 years) than in the West Med Sea (243 ± 87–386 ± 122 years) in both intermediate and deep layers (*t*-test, $p < 0.05$, Table S1). Turnover times for $FDOM_H$ in the deep East Med Sea were also relatively fast (153 ± 25–191 ± 54 years, Table S1).

4. Discussion

Water mass movement conveys $FDOM_H$, $CDOM_{UVA}$, and AOU signals from source areas to intermediate and deep layers of the dark marginal basin or global ocean along the hydrologic transport pathway. Thus, it is necessary to determine only the net in situ consumption of oxygen and in situ production/degradation signals for $CDOM_{UVA}$ and $FDOM_H$ to quantify their in situ production/degradation efficiencies in the dark layers (Catalá, Reche, Álvarez, et al., 2015; Catalá, Reche, Fuentes-Lema, et al., 2015). In the SCS and Japan Sea, net AOU and the net $CDOM_{UVA}$ and $FDOM_H$ signals were identified by a three-end-member mixing model and an OUR-inversed method, respectively (Text S1 and S2). In the Med Sea and global ocean, only archetypal AOU, $CDOM_{UVA}$, and $FDOM_H$ were reported (Catalá et al., 2018; Catalá, Reche, Álvarez, et al., 2015; Catalá, Reche, Fuentes-Lema, et al., 2015; Martínez-Pérez et al., 2019). As archetypal AOU represents the basin-scale magnitude of oxygen consumption between the source area and study sites in the global ocean and Med Sea, the in situ production/degradation efficiencies revealed by linear relationships between archetypal AOU and archetypal $CDOM_{UVA}$ and $FDOM_H$ were comparable to those estimated in the SCS and Japan Sea.

Differences in geomorphology controlled specific hydrological transport patterns within each dark marginal basin (Table S1). Strong downward ventilation in the Med and Japan Seas resulted in the warmest and coldest dark ocean temperatures, respectively. Importantly, ventilation also regulates the downward and lateral supply of labile carbon substrates (Lazzari et al., 2012; Ramondenc et al., 2016; Shen, Jiao, et al., 2020). For example, strong ventilation supplied a large DOC flux (9.2–13.8 g C m^{-2} yr^{-1}) to the deep East Med Sea, although POC export (0.5 g C m^{-2} yr^{-1}) was quite low from this area (Table S1). The negative relationships between net or archetypal $a_{CDOM}(254)$, peak T and AOU in the intermediate Japan and Med Seas reflect the existence of degradable DOM components in the two dark basins (Figures 2h, 2l, and 2m). In contrast, weak ventilation in the SCS results in rapid cycling of $a_{CDOM}(254)$ and $FDOM_T$ in the upper ocean instead of export to the intermediate layer (Hung et al., 2007; Liu et al., 2002). This results in a lack of correlations between $\Delta a_{CDOM}(254)$, Δpeak T, and ΔAOU in the intermediate SCS (Figures 2d and 2e). Deeper sill depths permit a large vertical temperature gradient and input of oxygen from the deep Northwest Pacific into the deep SCS. Therefore, hydrological transport processes in marginal basins regulate three key factors related to deep ocean organic matter transformations: temperature, supply of labile substrates and oxygen.

The generally positive relationship between the slope of $\Delta FDOM_H/\Delta AOU$ with dark ocean temperature (Figures 3a and 3b) infers the production of more recalcitrant $FDOM_H$ components at the expense of more degradable (labile) components when the temperature of the dark ocean increased. This finding is consistent with the classical Van't Hoff-Arrhenius relationship describing the influence of temperature on biochemical reaction rates (Arrhenius, 1889, Figure 3d). A higher supply of degradable substrates and/or higher average temperature contribute to faster turnover of $FDOM_H$ in the intermediate dark ocean than in the deep layer, and in dark marginal basins than in the open ocean. The positive shift of the slope (i.e., in situ production efficiency) relative to the low temperature in the dark intermediate Japan Sea may be ascribed to a substantially higher supply of labile/semi-labile substrates with a low apparent activation energy (Figures 3a and 3b, Table S1). For example, the apparent activation energy of microbial mineralization at 200 m in the Japan Sea estimated by ln(OUR)–$1/\theta$ relationship was the lowest value (Ea: 67.2 kJ mol^{-1}) among the three basins (Figure 3d). The rapid utilization of these non-recalcitrant substrates is consistent with the highest OUR (i.e., highest mineralization rate) among the three basins. This in turn could enhance the production efficiency of $FDOM_H$ in the cold dark Japan Sea.

At the lower temperature of the SCS and open ocean, both $a_{CDOM}(325)$ and $FDOM_H$ indicated a production pattern. When the temperature in the dark ocean became as high as the West Med Sea and intermediate East Med Sea (Table S1), the $a_{CDOM}(325)$ pattern indicated a change from production to degradation in the SCS and global ocean, whereas $FDOM_H$ retained its production signal. In the deep East Med Sea (>1,000 m), both $a_{CDOM}(325)$ and $FDOM_H$ were degraded and the DOM became extremely recalcitrant based on molecular-level indicators (Catalá et al., 2018; Martínez-Pérez et al., 2019). In total, these results reveal a temperature-related microbial degradation series for DOM components in the dark ocean, that is, $a_{CDOM}(325)$ was less recalcitrant than $FDOM_H$. In the dark SCS and open ocean, the lack of $a_{CDOM}(325)$ and $FDOM_H$ degradation implies that the availability of labile substrates does not limit microbial mineralization. This is

consistent with the low apparent activation energy in these two areas (Ea of intermediate SCS: 128 kJ mol^{-1}; Ea of open ocean: 138–165 kJ mol^{-1}, Figure 3d).

In the West Med Sea and intermediate East Med Sea, the higher apparent activation energy (258–1,733 kJ mol^{-1}, Figure 3d) and degradation of less recalcitrant DOM components (i.e., $a_{CDOM}(325)$) suggest rapid consumption (depletion) of labile substrates at higher temperatures, resulting in a "dark ocean labile-carbon limitation" status. This implies that a portion of the more recalcitrant carbon pool became a substrate for metabolism. The simultaneous degradation of $a_{CDOM}(325)$ and $FDOM_H$ and the high apparent activation energy (1,235 kJ mol^{-1}, Figure 3d) in the deep East Med Sea (>1,000 m) indicate a stronger deficit in the labile carbon pool. The supply of POC to the deep East Med Sea is rather negligible as POC export at 200 m was relatively small (Table S1). In contrast, there was downward input of DOC to the bottom layer of the deep East Med Sea (Figure 1d). The priming effect resulting from this DOC input might stimulate degradation of $FDOM_H$ in the dark ocean, contributing to the low DOC concentration (~36 μM) in the older, deep Med Sea waters (Santinelli et al., 2010). Thus, the integrated effects of temperature and substrate supply (quantity & quality) regulate the DOM reaction series in the dark ocean. Accompanying the increase of temperature and limitation of labile-carbon substrates was an increased recalcitrance of the remaining DOM pool in the dark ocean.

5. Implications

Climate model projections using a mid-range mitigation emissions scenario (RCP4.5) forecast temperature increases by 2,100 that are higher in the intermediate dark Japan Sea, SCS, and global ocean (0.79 ± 0.13°C, 0.57 ± 0.07°C, and 0.71 ± 0.05°C) than their respective deep layer (0.09 ± 0.04°C, 0.07 ± 0.05°C, and 0.18 ± 0.04°C) (Table S2). Hence, the response of DOM cycling to ocean warming will be most prominent in the intermediate layer. The projected increase in the net in situ $FDOM_H$ production rate was more strongly influenced by the projected increase in OUR rather than the projected increase of in situ $FDOM_H$ production efficiency (Table S3). Increases in both OUR (37% ± 9%) and in situ $FDOM_H$ production efficiency (peak A: 4.3% ± 0.7%, peak M: 2.6% ± 0.4%) were highest in the intermediate Japan Sea. As a result, the highest increase in microbial $FDOM_H$ production rates (43% ± 9% for peak A and 41% ± 9% for peak M) are projected to occur in the colder dark Japan Sea. Given the nonlinear relationship between ln(OUR) and $1/\theta$ (Figure 3d), this response of DOM production efficiency/rates to ocean warming was highly sensitive in this enclosed (sill depth <140 m), strongly ventilated, and high latitude dark marginal basin that contains ample semi-labile and semi-refractory DOM substrates (Kim et al., 2017). The warming response on $FDOM_H$ production efficiency in the deep Japan Sea could not be assessed due to the absence of temperature sensitivity data.

A simple mass balance model showed that rapid in situ production of $FDOM_H$ in the SCS is delivered to the open Pacific through the 2,500-m deep Luzon Strait along the intermediate layer (Tables S4 and S5), that is, the dark SCS acts as an "accelerated reactor" that increases the refractory carbon storage capacity of the global ocean interior. The projected temperatures in the dark SCS and global ocean at the end of 21st century do not approach the existing warm temperature status already present in the dark Med Sea, and therefore will not likely exceed the threshold to reverse the degradation signal for $a_{CDOM}(325)$ and $FDOM_H$. As the OUR is projected to increase by 12% ± 1%–16% ± 1% and 3% ± 2%–5% ± 1% in the intermediate and deep layers, respectively, there could be higher in situ $FDOM_H$ production rates in the intermediate layer (16% ± 1%–23% ± 1%) of the dark SCS and global ocean than in the deep layer (3% ± 2%–7% ± 1%) (Table S3). This would result in enhanced turnover and an increased inventory of these recalcitrant components in both the SCS and open ocean. While $a_{CDOM}(325)$ might show increased production at higher temperature, its inventory might not increase due to concomitant enhanced degradation (Figure 3c). Therefore, increased oxygen consumption and decreased labile carbon pools (e.g., 4% decrease of downward POC fluxes until 2090) in a future, warmer dark ocean (Yool et al., 2017; Lønborg et al., 2020), may initiate degradation of some semi-refractory components at longer timescales, thereby reducing total DOM storage.

The projected temperature increases through the end of the 21st century in the already warm dark West and East Med Seas (intermediate: 1.26 ± 0.08°C, 1.13 ± 0.10°C; deep: 0.21 ± 0.13°C and 0.25 ± 0.07°C) were much higher (Table S2). As a result, the projected OUR in the dark West and East Med Seas could increase

by 178% and 23%. This outcome is unlikely due to the ultra-refractory nature of the DOM (i.e., compounds with a significant increase in molecular weight, oxygenation, and degradation index) in the current Med Sea. Thus, microbial metabolism will become substrate limited due to the low availability of degradable organic matter in a future, warmer Med Sea (Martínez-Pérez et al., 2017). However, this could induce enhanced degradation of more recalcitrant components resulting in a decrease of the RDOM inventory in a future, warmer Med Sea. For example, the in situ degradation rate of $a_{CDOM}(325)$ in a future, warmer dark Med Sea and $FDOM_H$ in the deep East Med Sea could increase 37% ± 9% and 17% ± 7% by 2100 (Table S3), if assuming the in situ degradation efficiencies of these components remain at their current levels. This emphasizes the critical role of organic carbon cycling in the warm dark ocean during past climate alterations regardless of its oxygen state, as mineralization-related $FDOM_H$ accumulation was independent of the oxidizing agent (i.e., oxygen or sulfate) (Margolin et al., 2018). Thus, a decrease in the DOM inventory by enhanced microbial mineralization (producing CO_2) in a warmer dark ocean may create a positive feedback in response to global climate change.

Conflict of Interest

The authors declare no conflicts of interest relevant to this study.

Data Availability Statement

The data are available in the Mendeley Data Repository (https://data.mendeley.com/datasets/cvhz9rk4gw/1).

Acknowledgments
This work was jointly supported by National Natural Science Foundation of China (41876083) and the Senior User Project of R/V KEXUE (KEXUE2017G11, KEXUE2018G03). Data and samples were collected onboard the R/V Dongfanghong II (NORC2015-05 cruise) and R/V Tan Kah Kee (NORC2018-05 cruise) supported by NSFC Shiptime Sharing Project. The authors are grateful to the caption, crew, and other technical staff for their help during the cruises. The authors thank Dr. Piotr Kowalczuk and an anonymous reviewer for their insightful comments.

References

Arrhenius, S. (1889). Uber die reaktionsgeschwindigkeit bei der inversion von rohrzucker durch sauren. *Zeitschrift für Physikalische Chemie*, *4*, 226–248. https://doi.org/10.1515/zpch-1889-0416

Benson, B. B., & Krause, D. (1984). The concentration and isotopic fractionation of oxygen dissolved in fresh-water and seawater in equilibrium with the atmosphere. *Limnology and Oceanography*, *29*(3), 620–632. https://doi.org/10.4319/lo.1984.29.3.0620

Brewer, P. G., & Peltzer, E. T. (2017). Depth perception: The need to report ocean biogeochemical rates as functions of temperature, not depth. *Philosophical Transactions of the Royal Society A*, *375*, 20160319. https://doi.org/10.1098/rsta.2016.0319

Cao, Z. M., & Dai, M. H. (2011). Shallow-depth $CaCO_3$ dissolution: Evidence from excess calcium in the South China Sea and its export to the Pacific Ocean. *Global Biogeochemical Cycles*, *25*, GB2019. https://doi.org/10.1029/2009gb003690

Catalá, T. S., Martínez-Pérez, A. M., Nieto-Cid, M., Álvarez, M., Otero, J., Emelianov, M., et al. (2018). Dissolved organic matter (DOM) in the open Mediterranean Sea. I. Basin-wide distribution and drivers of chromophoric DOM. *Progress in Oceanography*, *165*, 35–51. https://doi.org/10.1016/j.pocean.2018.05.002

Catalá, T. S., Reche, I., Álvarez, M., Khatiwala, S., Guallart, E. F., Benítez-Barrios, V. M., et al. (2015). Water mass age and aging driving chromophoric dissolved organic matter in the dark global ocean. *Global Biogeochemical Cycles*, *29*(7), 917–934. https://doi.org/10.1002/2014gb005048

Catalá, T. S., Reche, I., Fuentes-Lema, A., Romera-Castillo, C., Nieto-Cid, M., Ortega-Retuerta, E., et al. (2015). Turnover time of fluorescent dissolved organic matter in the dark global ocean. *Nature Communications*, *6*, 5986.

Chen, C. T. A., Wang, S. L., Wang, B. J., & Pai, S. C. (2001). Nutrient budgets for the South China Sea basin. *Marine Chemistry*, *75*(4), 281–300. https://doi.org/10.1016/s0304-4203(01)00041-x

Cheng, L. J., Trenberth, K. E., Fasullo, J., Boyer, T., Abraham, J., & Zhu, J. (2017). Improved estimates of ocean heat content from 1960 to 2015. *Science Advances*, *3*(3), e1601545. https://doi.org/10.1126/sciadv.1601545

Coble, P. G. (1996). Characterization of marine and terrestrial DOM in seawater using excitation emission matrix spectroscopy. *Marine Chemistry*, *51*(4), 325–346. https://doi.org/10.1016/0304-4203(95)00062-3

Coble, P. G., Spencer, R. G. M., Baker, A., & Reynolds, D. M. (2014). *Aquatic organic matter fluorescence* (pp. 75–122). Cambridge University Press.

Hansell, D. A. (2013). Recalcitrant dissolved organic carbon fractions. *Annual Review of Marine Science*, *5*, 421–445. https://doi.org/10.1146/annurev-marine-120710-100757

Hansell, D. A., Carlson, C. A., Repeta, D. J., & Schlitzer, R. (2009). Dissolved organic matter in the ocean a controversy stimulates new insights. *Oceanography*, *22*(4), 202–211. https://doi.org/10.5670/oceanog.2009.109

Hayase, K., & Shinozuka, N. (1995). Vertical distribution of fluorescent organic-matter along with AOU and nutrients in the equatorial Central Pacific. *Marine Chemistry*, *48*(3–4), 283–290. https://doi.org/10.1016/0304-4203(94)00051-e

Hung, J. J., Wang, S. M., & Chen, Y. L. (2007). Biogeochemical controls on distributions and fluxes of dissolved and particulate organic carbon in the Northern South China Sea. *Deep Sea Research Part II: Topical Studies in Oceanography*, *54*(14), 1486–1503. https://doi.org/10.1016/j.dsr2.2007.05.006

Jiao, N., Herndl, G. J., Hansell, D. A., Benner, R., Kattner, G., Wilhelm, S. W., et al. (2010). Microbial production of recalcitrant dissolved organic matter: Long-term carbon storage in the global ocean. *Nature Reviews Microbiology*, *8*(8), 593–599. https://doi.org/10.1038/nrmicro2386

Karstensen, J., & Tomczak, M. (1998). Age determination of mixed water masses using CFC and oxygen data. *Journal of Geophysical Research: Oceans*, *103*(C9), 18599–18609. https://doi.org/10.1029/98jc00889

Kim, D., Choi, M.-S., Oh, H.-Y., Song, Y.-H., Noh, J.-H., & Kim, K. H. (2011). Seasonal export fluxes of particulate organic carbon from $^{234}Th/^{238}U$ disequilibrium measurements in the Ulleung Basin1 (Tsushima Basin) of the East Sea1 (Sea of Japan). *Journal of Oceanography*, *67*(5), 577–588. https://doi.org/10.1007/s10872-011-0058-8

Kim, I. N., Min, D. H., & Lee, T. S. (2010). Estimates of basin-specific oxygen utilization rates (OURs) in the East Sea (Sea of Japan). *Journal of the Korean Society of Oceanography*, *15*(2), 86–96.

Kim, J., & Kim, G. (2016). Significant anaerobic production of fluorescent dissolved organic matter in the deep East Sea (Sea of Japan). *Geophysical Research Letters*, *43*(14), 7609–7616. https://doi.org/10.1002/2016gl069335

Kim, K., Kim, K. R., Kim, Y. G., Cho, Y. K., Kang, D. J., Takematsu, M., et al. (2004). Water masses and decadal variability in the East Sea (Sea of Japan). *Progress in Oceanography*, *61*(2–4), 157–174. https://doi.org/10.1016/j.pocean.2004.06.003

Kim, T. H., Kim, G., Shen, Y., & Benner, R. (2017). Strong linkages between surface and deep-water dissolved organic matter in the East/Japan Sea. *Biogeosciences*, *14*(9), 2561–2570. https://doi.org/10.5194/bg-14-2561-2017

Lazzari, P., Solidoro, C., Ibello, V., Salon, S., Teruzzi, A., Béranger, K., et al. (2012). Seasonal and inter-annual variability of plankton chlorophyll and primary production in the Mediterranean Sea: A modelling approach. *Biogeosciences*, *9*(1), 217–233. https://doi.org/10.5194/bg-9-217-2012

Levitus, S., Antonov, J. I., Boyer, T. P., Baranova, O. K., Garcia, H. E., Locarnini, R. A., et al. (2012). World ocean heat content and thermosteric sea level change (0–2000 m), 1955–2010. *Geophysical Research Letters*, *39*, L10603. https://doi.org/10.1029/2012gl051106

Liu, K. K., Chao, S. Y., Shaw, P. T., Gong, G. C., Chen, C. C., & Tang, T. Y. (2002). Monsoon-forced chlorophyll distribution and primary production in the South China Sea: Observations and a numerical study. *Deep Sea Research Part I: Oceanographic Research Papers*, *49*(8), 1387–1412. https://doi.org/10.1016/s0967-0637(02)00035-3

Liu, Z. Q., & Gan, J. P. (2017). Three-dimensional pathways of water masses in the South China Sea: A modeling study. *Journal of Geophysical Research: Oceans*, *122*(7), 6039–6054. https://doi.org/10.1002/2016jc012511

Lønborg, C., & Álvarez-Salgado, X. A. (2014). Tracing dissolved organic matter cycling in the eastern boundary of the temperate North Atlantic using absorption and fluorescence spectroscopy. *Deep Sea Research Part I: Oceanographic Research Papers*, *85*, 35–46.

Lønborg, C., Álvarez-Salgado, X. A., Letscher, R. T., & Hansell, D. A. (2018). Large stimulation of recalcitrant dissolved organic carbon degradation by increasing ocean temperatures. *Frontiers in Marine Science*, *4*, 436.

Lønborg, C., Carreira, C., Jickells, T., & Álvarez-Salgado, X. A. (2020). Impacts of global change on ocean dissolved organic carbon (DOC) cycling. *Frontiers in Marine Science*, *7*, 466.

Margolin, A. R., Gonnelli, M., Hansell, D. A., & Santinelli, C. (2018). Black Sea dissolved organic matter dynamics: Insights from optical analyses. *Limnology and Oceanography*, *63*(3), 1425–1443. https://doi.org/10.1002/lno.10791

Martínez-Pérez, A. M., Catalá, T. S., Nieto-Cid, M., Otero, J., Álvarez, M., Emelianov, M., et al. (2019). Dissolved organic matter (DOM) in the open Mediterranean Sea. II: Basin-wide distribution and drivers of fluorescent DOM. *Progress in Oceanography*, *170*, 93–106.

Martínez-Pérez, A. M., Osterholz, H., Nieto-Cid, M., Álvarez, M., Dittmar, T., & Álvarez-Salgado, X. A. (2017). Molecular composition of dissolved organic matter in the Mediterranean Sea. *Limnology and Oceanography*, *62*(6), 2699–2712. https://doi.org/10.1002/lno.10600

Min, D. H., Kim, K.-R., & Weiss, R. F. (2002). Decadal-scale changes of ventilation rates in the East Sea (Sea of Japan): A study by the chlorofluorocarbons and a simple model. In *CREAMS/PICES Symposium, Seoul, Korea*.

Qu, T. D., Girton, J. B., & Whitehead, J. A. (2006). Deepwater overflow through Luzon Strait. *Journal of Geophysical Research: Oceans*, *111*(C1). https://doi.org/10.1029/2005jc003139

Ramondenc, S., Madeleine, G., Lombard, F., Santinelli, C., Stemmann, L., Gorsky, G., & Guidi, L. (2016). An initial carbon export assessment in the Mediterranean Sea based on drifting sediment traps and the Underwater Vision Profiler data sets. *Deep Sea Research Part I: Oceanographic Research Papers*, *117*, 107–119. https://doi.org/10.1016/j.dsr.2016.08.015

Santinelli, C. (2015). DOC in the Mediterranean Sea. In D. A. Hansell & C. A. Carlson (Eds.), *Biogeochemistry of marine dissolved organic matter* (2nd ed., pp. 579–608). Academic Press. https://doi.org/10.1016/b978-0-12-405940-5.00013-3

Santinelli, C., Nannicini, L., & Seritti, A. (2010). DOC dynamics in the meso and bathypelagic layers of the Mediterranean Sea. *Deep Sea Research Part II: Topical Studies in Oceanography*, *57*(16), 1446–1459. https://doi.org/10.1016/j.dsr2.2010.02.014

Shen, J. M., Jiao, N., Dai, M., Wang, H., Qiu, G., Chen, J., et al. (2020). Laterally transported particles from margins serve as a major carbon and energy source for dark ocean ecosystems. *Geophysical Research Letters*, *47*(18). https://doi.org/10.1029/2020gl088971

Shen, Y., & Benner, R. (2020). Molecular properties are a primary control on the microbial utilization of dissolved organic matter in the ocean. *Limnology and Oceanography*, *65*, 1061–1071. https://doi.org/10.1002/lno.11369

Soto-Navarro, J., Jordá, G., Amores, A., Cabos, W., Somot, S., Sevault, F., et al. (2020). Evolution of Mediterranean Sea water properties under climate change scenarios in the Med-CORDEX ensemble. *Climate Dynamics*, *54*(3–4), 2135–2165. https://doi.org/10.1007/s00382-019-05105-4

Stöven, T., & Tanhua, T. (2014). Ventilation of the Mediterranean Sea constrained by multiple transient tracer measurements. *Ocean Science*, *10*(3), 439–457. https://doi.org/10.5194/os-10-439-2014

Swan, C. M., Siegel, D. A., Nelson, N. B., Carlson, C. A., & Nasir, E. (2009). Biogeochemical and hydrographic controls on chromophoric dissolved organic matter distribution in the Pacific Ocean. *Deep Sea Research Part I: Oceanographic Research Papers*, *56*(12), 2175–2192. https://doi.org/10.1016/j.dsr.2009.09.002

Tanaka, K., Kuma, K., Hamasaki, K., & Yamashita, Y. (2014). Accumulation of humic-like fluorescent dissolved organic matter in the Japan Sea. *Scientific Reports*, *4*, 5292. https://doi.org/10.1038/srep05292

Wang, C., Guo, W. D., Li, Y., Stubbins, A., Li, Y. Z., Song, G. D., et al. (2017). Hydrological and biogeochemical controls on absorption and fluorescence of dissolved organic matter in the Northern South China Sea. *Journal of Geophysical Research-Biogeosciences*, *122*(12), 3405–3418. https://doi.org/10.1002/2017jg004100

Wang, C., Li, Y., Li, Y., Zhou, H., Stubbins, A., Dahlgren, R. A., et al. (2021). Dissolved organic matter dynamics in the epipelagic Northwest Pacific low-latitude western boundary current system: Insights from optical analyses. *Journal of Geophysical Research: Oceans*, *126*, e2021JC017458. https://doi.org/10.1029/2021jc017458

Watanabe, Y. W., Watanabe, S., & Tsunogai, S. (1991). Tritium in the Japan Sea and the renewal time of the Japan Sea deep water. *Marine Chemistry*, *34*(1), 97–108. https://doi.org/10.1016/0304-4203(91)90016-p

Wu, K., Dai, M. H., Chen, J. H., Meng, F. F., Li, X. L., Liu, Z. Y., et al. (2015). Dissolved organic carbon in the South China Sea and its exchange with the Western Pacific Ocean. *Deep Sea Research Part II: Topical Studies in Oceanography*, *122*, 41–51. https://doi.org/10.1016/j.dsr2.2015.06.013

Yamashita, Y., & Tanoue, E. (2008). Production of bio-refractory fluorescent dissolved organic matter in the ocean interior. *Nature Geoscience*, *1*(9), 579–582. https://doi.org/10.1038/ngeo279

Yool, A., Martin, A. P., Anderson, T. R., Bett, B. J., Jones, D. O. B., & Ruhl, H. A. (2017). Big in the benthos: Future change of seafloor community biomass in a global, body size-resolved model. *Global Change Biology*, *23*(9), 3554–3566. https://doi.org/10.1111/gcb.13680

Zhu, Y. H., Sun, J. C., Wang, Y. G., Li, S. J., Xu, T. F., Wei, Z. X., & Qu, T. (2019). Overview of the multi-layer circulation in the South China Sea. *Progress in Oceanography*, *175*, 171–182. https://doi.org/10.1016/j.pocean.2019.04.001